Dalton Transactions

ROYAL SOCIETY OF CHEMISTRY

PAPER

View Article Online
View Journal | View Issue

Check for updates

Cite this: *Dalton Trans.*, 2024, **53**, 7012

Synthesis, polymorphism, and shape complementarity-induced co-crystallization of hexanuclear Co(II) clusters capped by a flexible heteroligand shell†

Michał Terlecki, *[a] Arkadiusz Kornowicz, [b] Kornel Sacharczuk,[a] Iwona Justyniak [b] and Janusz Lewiński *[a,b]

Received 28th January 2024,
Accepted 27th March 2024

DOI: 10.1039/d4dt00261j

rsc.li/dalton

Polymorphism and co-crystallization have gradually gained attention as new tools in the development of modern crystalline functional materials. However, the study on the selective self-assembly of metal clusters into multicomponent crystals is still in its infancy. Herein, we present the synthesis and characterization of two new heteroleptic hydroxido-acetato and acetato Co(II) clusters $[Co_6(OH)_2(OAc)_4(pyret)_6]$ (**1**) and $[Co_6(OAc)_6(pyret)_6]$ (**2**) incorporating auxiliary 2-pyrrolidinoethoxylate (*pyret*) ligands. On this occasion, we revealed that the commonly used thermal procedure for dehydration of cobalt(II) acetate leads to a reagent comprising substantial contamination by cobalt hydroxido moieties. Comprehensive structural analysis of new compounds demonstrated intriguing crystal structure diversity of hydroxido-acetato cluster **1**, which represents a rare example of both conformational and packing polymorphism in one compound, originating from the flexibility of organic *O,N*-ligands in the secondary coordination sphere. Furthermore, both clusters exhibit an interesting propensity for the selective formation of co-crystals **1·2** driven mainly by van der Waals forces and specific shape complementarity between co-formers.

Open Access Article. Published on 28 March 2024. Downloaded on 1/23/2026 5:57:32 PM.
This article is licensed under a Creative Commons Attribution 3.0 Unported Licence.

Introduction

The introduction of organic or inorganic additives either deliberately as materials dopants[1,2] or serendipitously as impurities in reaction systems[3–5] may significantly alter the characteristics of the products, leading to their new unique properties. Notably, many groundbreaking discoveries have been initiated by accidental contamination of the reaction systems, such as the development of Ziegler–Natta catalysts for olefin polymerization originated from the observation of catalytic effects of nickel impurities from the steel reaction vessel,[6] the first syntheses of ferrocene by passing hot cyclopentadiene vapor through an iron pipe,[7] or even development of the first controllable synthesis of colloidal quantum dots by Bawendi, who used old batches of n-butylphosphine contaminated by its oxidated form.[8] Although serendipity is an important part of initial discoveries paving the way for new research directions,[4] subsequent rationally designed experiments conducted in a controlled and reproducible manner are crucial for the understanding of new phenomena.[9,10] In this view, the proper purification and characterization of starting well-defined reagents and solvents, which may be contaminated by i.a. residuals from synthesis, different isomers, or products of degradation due to improper or prolonged storage, is of particular importance.[11]

Cobalt(II) carboxylates are important catalysts and reagents in organic synthesis.[12,13] Furthermore, they found wide applications as efficient precursors of functional materials including cobalt oxide nanocrystals[14] and metal–organic frameworks.[15–17] On the other hand, polynuclear cobalt clusters are of longstanding interest, owing to their promising magnetic[18,19] and catalytic properties,[20] as well as their applications as metalloenzyme models.[21–23] In this view, carboxylate-supported systems are of particular interest due to the versatility of binding modes of carboxylate ligands,[19,24] the propensity of carboxylate bridges to mediate magnetic interactions,[19,23–25] and the prevalence of carboxylic moieties in biological systems.[21,26,27] However, cobalt carboxylates exhibit extensive stoichiometric and structural diversity and the development of reliable synthetic routes to oligomeric cobalt carboxylato clusters with controllable structure and reactivity is highly challenging.[19] Even simple homoleptic

[a]*Faculty of Chemistry, Warsaw University of Technology, Noakowsiego 3, 00-664 Warsaw, Poland. E-mail: michal.terlecki@pw.edu.pl, janusz.lewinski@pw.edu.pl*
[b]*Institute of Physical Chemistry, Polish Academy of Sciences, Kasprzaka 44/52, 01-224 Warsaw, Poland*

†Electronic supplementary information (ESI) available: Crystal structures analysis, PXRD and TGA measurements, and color change during Co(II) acetate purification. CCDC 2321233–2321237. For ESI and crystallographic data in CIF or other electronic format see DOI: https://doi.org/10.1039/d4dt00261j

This journal is © The Royal Society of Chemistry 2024

Open Access Article. Published on 28 March 2024. Downloaded on 1/23/2026 5:57:32 PM. This article is licensed under a Creative Commons Attribution 3.0 Unported Licence.

Co(II) carboxylates form diverse hydrates that can be easily transformed into various cobalt oxido- and hydroxido-carboxylato clusters, which structure is strongly affected by the reaction conditions.[28] Further control over the structure of cobalt carboxylates may be achieved by the introduction of auxiliary stabilizing neutral or anionic ligands that paved the way for a wide range of heteroleptic clusters with nuclearity ranging from mononuclear to approaching the size of nanoparticles.[19,29] Notably, these organic ligands also participate in intermolecular interactions governing the self-assembly of metal clusters in the crystal lattice. Thus, the utilization of new compounds for the stabilization of Co(II) complexes is a promising strategy in the development of new cobalt clusters-based functional materials.

The physicochemical characteristic of crystalline materials is determined not only by the molecular structure of building units but also by their packing in the crystal lattice. Hence, the ability of some chemical compounds to the formation of various polymorphs can be used as a convenient tool to fine-tune their properties.[30–32] Generally, molecular polymorphism can be classified into two main categories: packing polymorphism when the same molecule can assembled into various crystal lattices, and conformational polymorphism, which occurs when a molecule can exist in crystals in two or more different conformations. Both these phenomena are related to different features of molecules, *i.e.* their self-assembly properties and molecular flexibility, respectively, and rarely are manifest in one compound simultaneously.[33] Another way to tune the physicochemical characteristic of crystalline solids is the formation of multicomponent crystals, which often exhibit novel properties, differing from those of simple physical mixtures of co-formers.[34–41] In recent years, both polymorphism and co-crystalization have emerged as useful tools in the development of modern crystalline functional materials.[37,40,42–49] Especially, co-crystallization of various organic molecules led to improved ferroelectric, phosphorescent, or ambipolar charge transport properties of organic-based materials,[44,49] while the combination of various building blocks allowed for fine-tuning porosity and physicochemical properties of hydrogen-[50–52] and halogen-bonded[53–55] organic frameworks as well as porous organic cages.[56,57] However, examples of the co-crystallization between metal complexes or polynuclear metal clusters with hybrid organic–inorganic character are much less common, and investigations on their selective multicomponent self-assembly are still in their infancy.[40,41,58–60] Furthermore, while the selective formation of co-crystals directed by specific noncovalent interactions between co-formers is widely recognized, similar phenomena based on specific shape and/or size complementarity of building units, are rarely explored.[61]

Based on our longstanding experience in the design and development of synthetic approaches for main-group and transition metal multinuclear clusters[62–69] as well as the studies on the noncovalent interactions-driven self-assembly of metal complexes,[63,64,68,70–74] herein, we present the synthesis and comprehensive structural characterization of two new heteroleptic hydroxido-acetato and acetato Co(II) clusters $[Co_6(OH)_2(OAc)_4(pyret)_6]$ (**1**) and $[Co_6(OAc)_6(pyret)_6]$ (**2**) incorporating an auxiliary 2-pyrrolidinoethoxylate (*pyret*) ligand. Remarkably, the proper purification of a starting Co(II) acetate reagent played a pivotal role in the selective formation of clusters **1** or **2**. Comprehensive structural analysis of new compounds demonstrated intriguing crystal structure diversity of hydroxido-acetato cluster **1**, which represents a rare example of both conformational and packing polymorphism in one compound. Furthermore, both clusters exhibit an interesting propensity for the selective formation of co-crystals **1·2** driven mainly by van der Waals forces and specific shape complementarity between co-formers.

Results and discussion

Development of synthetic procedures for hydroxido-acetato and acetate clusters, $[Co_6(OH)_2(OAc)_4(pyret)_6]$ (1) and $[Co_6(OAc)_6(pyret)_6]$ (2), and their co-crystallization

Numerous previous studies showed that the application of auxiliary stabilizing ligands enables the control over the structure and nuclearity of cobalt(II) acetato clusters, however, still in a highly unpredictable manner.[19] With this in mind, we selected 2-pyrrolidinoethoxylate (*pyret*) as a model *O,N*-bidentate ligand in order to study their role in the stabilization of cobalt(II) carboxylates. Our primary attempts to isolate well-defined crystalline products *via* the direct reaction of $Co(OAc)_2$ or $Co(OAc)_2{\cdot}4H_2O$ with *pyret*-H afforded an intractable mixture of products. Thus, in the next step, we turned our attention to transmetalation reactions utilizing potassium salts of ligand (*pyret*-K), which, in our previous works, proved to be an effective strategy to introduce various anionic organic ligands to transition metal coordination compounds.[68,75,76] This approach paved the way for the efficient synthesis of new heteroleptic hydroxido-acetato and hexameric acetato clusters **1** and **2**, respectively. Further experiments revealed an interesting predisposition of both compounds to the formation of a stoichiometric co-crystal **1·2**.

Synthesis of clusters 1 and 2. Reactions of *pyret*-K with as-received commercial anhydrous $Co(OAc)_2$ led repeatedly to high-quality violet-pink crystals of **1** (Fig. 1a, path A), which were characterized by single-crystal and powder X-ray diffraction (SC-XRD and PXRD), Fourier-transform infrared spectroscopy (FTIR) and elemental analysis (for details see the Experimental section (ES) and ESI†). Interestingly, SC-XRD measurements on various selected crystals revealed that cluster **1** crystallizes as a mixture of three different polymorphic forms (*vide infra*), which were formed simultaneously and unselectively, regardless of crystallization conditions like solution concentration or temperature (Fig. S6†).

Cluster **2** can be described as a heteroleptic hexameric cobalt carboxylate complex $[Co_6(OAc)_6(pyret)_6]$ (**2**) with two acetate anions substituted by hydroxide groups. Proligand *pyret*-H was carefully purified by distillation over CaH_2 prior to the preparation of its potassium salt *via* the reaction with pot-

Open Access Article. Published on 28 March 2024. Downloaded on 1/23/2026 5:57:32 PM.
This article is licensed under a Creative Commons Attribution 3.0 Unported Licence.

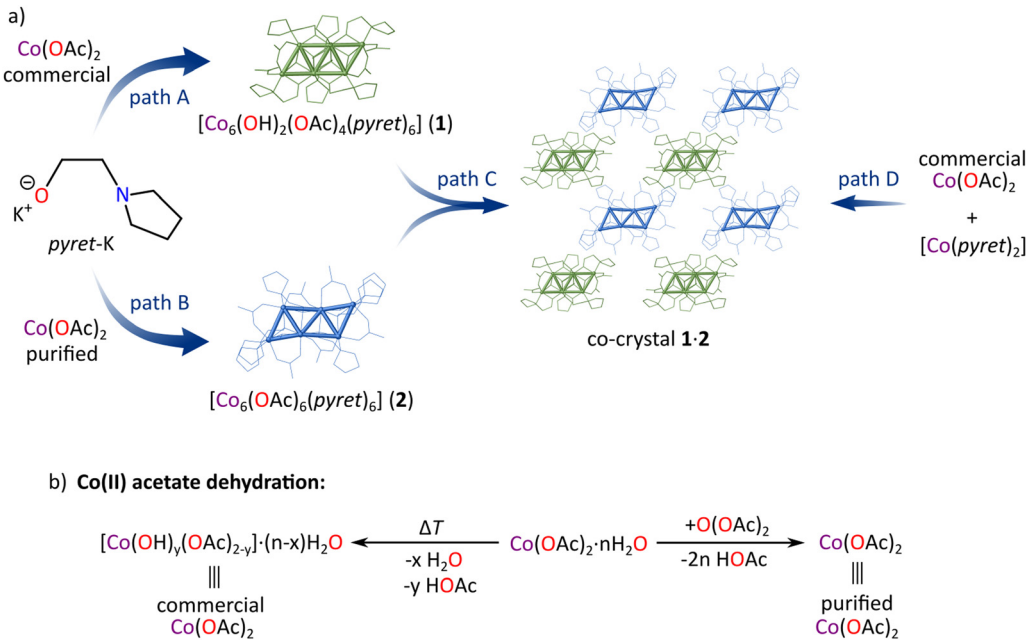

Fig. 1 Schematic representation of: (a) the preparation of monocomponent crystals of **1** and **2** and co-crystal **1·2**, (b) dehydration of cobalt(II) acetate *via* thermal and acetic anhydride-based procedures.

assium bis(trimethylsilyl)amide (KHMDS) (see ES). Thus, the commercial anhydrous $Co(OAc)_2$ was likely the source of OH groups in **1**. Next, in order to obtain the initial complex **2**, we designed a new procedure for the purification of $Co(OAc)_2$, involving its treatment with acetic anhydride at 90 °C (*vide infra*). The reaction of the as-purified anhydrous $Co(OAc)_2$ with *pyret*-K afforded high-quality violet-pink crystals of **2** in high yield (Fig. 1a, path B), which were characterized by SC-XRD, FTIR, and elemental analysis (for details see ES and ESI†).

Effect of the purity of starting cobalt(II) acetate on the reaction outcome. Intrigued by the profound role of the purity of anhydrous $Co(OAc)_2$ in the synthesis of **1** and **2**, we take a closer look at the differences in the composition of starting reagents. The anhydrous $Co(OAc)_2$ purchased from Sigma-Aldrich (99.99% trace metals basis, ≤5% water) was purple-violet in color. However, pure crystals of $[Co_5(OAc)_{10}]_n$ are expected to be pink, which is typical for Co(II) ions in the octahedral coordination environment.[77] A change of color from pink to blue was previously observed upon thermal dehydration of Co(II) salts associated with the conversion of the cobalt coordination sphere from O_h to T_d geometry.[78] Thus, we assumed that the provided commercial $Co(OAc)_2$ was likely dehydrated by annealing under reduced pressure, which is a commonly applied procedure.[79] However, according to some previous studies on the thermal decomposition of $Co(OAc)_2{\cdot}4H_2O$, in this case, the elimination of H_2O molecules may be accompanied by the competitive elimination of acetic acid, leading to the generation of Co–OH moieties (Fig. 1b).[80,81] To confirm that, we performed the thermal dehydration of $Co(OAc)_2{\cdot}4H_2O$ by heating at 120 °C under reduced pressure by 12 h obtaining a violet powder product. The PXRD analysis revealed the presence of an unidentified crystal phase in both the as-prepared and commercial reagents (Fig. S5†), while the elemental analysis showed their similar composition, indicating on general formulas as $[Co(OH)_{0.28}(OAc)_{1.72}]{\cdot}0.12H_2O$ and $[Co(OH)_{0.34}(OAc)_{1.66}]{\cdot}0.70H_2O$, respectively (see ES). Both of them in the reaction with *pyret*-K give the same product **1** with a high yield. The presence of water and/or OH groups in both reagents was also indicated by thermogravimetric (TGA) analysis (see, ESI, Fig. S2 and S3†). Interestingly, the received Co : OH molar ratio in thermally treated cobalt(II) acetate is close to 3, which may suggest that the $\{Co_3(\mu_3\text{-}OH)\}$ units observed in the molecular structure of **1** (*vide infra*) are already present in the starting reagent. In turn, acetic anhydride easily reacts with both H_2O molecules and Co–OH groups giving acetic acid and cobalt acetate species, which we used to efficiently dehydrate $Co(OAc)_2{\cdot}4H_2O$ or purify commercial $[Co(OH)_{0.34}(OAc)_{1.66}]{\cdot}0.70H_2O$ reagents leading to pure anhydrous $Co(OAc)_2$ (Fig. 1b), as evidenced by elemental, PXRD, and TGA analysis (see ES and ESI, Fig. S4 and S5†).

Co-crystallization of 1 and 2. During our studies, we also attempted to minimize the OH^-/H_2O impurities introduced to the reaction system in cobalt(II) acetate reagent by applying the Co(II) salt of *pyret* as a source of both Co(II) and *pyret* ligands. Interestingly, from the equimolar reaction of $Co(pyret)_2$ with commercial Co(II) acetate we isolated co-crystals of **1** and **2** with 1 : 1 stoichiometry, which were characterized by SC-XRD and elemental analysis (Fig. 1a, path D). The application of Co(*pyret*)$_2$ reduced by half the number of OH^-/H_2O impurities introduced by commercial $Co(OAc)_2$, which likely led to the simultaneous formation of equimolar amounts of **1** and **2** in the reaction mixture and their subsequent co-crystallization.

 This journal is © The Royal Society of Chemistry 2024

Open Access Article. Published on 28 March 2024. Downloaded on 1/23/2026 5:57:32 PM. This article is licensed under a Creative Commons Attribution 3.0 Unported Licence.

Co-crystals **1·2** were also successfully obtained in high yield by controlled crystallization *via* slow diffusion of hexane vapor to THF solution containing the equimolar mixture of presynthesized clusters **1** and **2** (Fig. 1a and S7,† path C).

Analysis of the crystal structures of 1, 2, and 1·2

Crystal structure and polymorphism of 1. Cluster **1** crystallizes in three polymorphic forms named phase α, β, and γ. Phases α and β adopt similar $P2_1/n$ and $P2_1/c$ space groups, respectively, but differ significantly in the supramolecular arrangement of molecules in the crystal lattice (for the description of supramolecular structures, *vide infra*). In turn, phase γ, which crystallizes in the $Pca2_1$ space group, shows similar crystal packing to phase β but differs in the conformation of *pyret* ligands in the secondary coordination sphere of **1**. The respective conformers of **1** in phases α and β and phase γ are hereafter termed $\mathbf{1^a}$ and $\mathbf{1^b}$. The molecular structure of **1** is centrosymmetric and comprises a parallelogram Co_6 core composed of four edge-fused $\{Co_3\}$ triangles, each containing central μ_3-bridging oxygen atom provided either by μ_3-$\kappa^2(O,N)$:$\kappa^1(O)$:$\kappa^1(O)$ *pyret* ligands or μ_3-OH groups (Fig. 2a). The shorter edge of the parallelogram core is coordinated by two acetate anions, one acting as a bridging μ_2 ligand and the other adopting monodentate κ^1 coordination mode supported by a hydrogen bond with the μ_3-OH group at the center of the two outermost triangular units of the Co_6 core. The resulting hydroxido-acetato $[Co_6(OH)_2(OAc)_4]^{6+}$ cluster is stabilized by six monoanionic O,N-bidentate *pyret* ligands, two with the μ_3-$\kappa^2(O,N)$:$\kappa^1(O)$:$\kappa^1(O)$ coordination mode located above and below the plane of Co_6 core and four with μ_2-$\kappa^2(O,N)$:$\kappa^1(O)$ coordination mode bonded at the longer edges of the Co_6 parallelogram. Four Co centers at the vertices of the parallelogram core adopt an O_4N coordination sphere with highly deformed geometries varying between trigonal bipyramid and square pyramid (for details see ESI†), while the other two Co centers at the middle of the longer parallelogram edges are in a deformed octahedral O_5N coordination environment. Most of the Co–O bonds are in the range of 1.947–2.188 Å and only those between OH groups and octahedral Co centers are longer reaching 2.238–2.253 Å. All the Co–N bonds are in the range of 2.216–2.281 Å.

The existence of conformers $\mathbf{1^a}$ and $\mathbf{1^b}$ is a consequence of conformational movements of organic backbones in the secondary coordination sphere of **1**, resulting mainly from the isomerism of pentanuclear $\{CoOC_\alpha C_\beta N\}$ macrocycles formed by the chelating *O,N*-bidentate ligands (Fig. 2c). This type of five-membered ring can adopt one of 20 various conformers, which can be classified as either twist (*T*) or envelope (*E*) by analogy with furanose rings.[82] The transition from $\mathbf{1^a}$ to $\mathbf{1^b}$ is associated with the conformational movement of carbon atoms in the β position of aminoalkoxylate backbone in four of six *pyret* ligands. Especially, the $\{CoOC_\alpha C_\beta N\}$ macrocycle formed by one of μ_3-$\kappa^2(O,N)$:$\kappa^1(O)$:$\kappa^1(O)$-*pyret* ligands in conformer $\mathbf{1^a}$ adopts N-*endo* envelope conformation ${}_{N}E$, while in conformer $\mathbf{1^b}$ is transformed to C_α-*endo* envelope conformation ${}_{C_\alpha}E$ (Fig. 2c, frame A). Simultaneously, the conformation of the $\{CoOC_\alpha C_\beta N\}$ macrocycle formed by one of the μ_2-$\kappa^2(O,N)$:$\kappa^1(O)$-*pyret* ligands change from C_β-*endo* envelope ${}_{C_\beta}E$ in $\mathbf{1^a}$ into C_β-*exo* envelope ${}^{C_\beta}E$ in $\mathbf{1^b}$ (Fig. 2c, frame B). This transition affects the orientation of pyrrolidine group that in conformer $\mathbf{1^b}$ is faced toward the H-bonded carboxylate anion, which, likely due to steric hindrance, triggers its concomitant conformational transformation from N-*endo* to N-*exo* envelope. As the molecular structure of **1** is centrosymmetric, the mirrored transitions occur on the other side of the molecule. The changes in the conformation of the $\{CoOC_\alpha C_\beta N\}$ macrocycles are accompanied by small successive movements of other elements of the secondary coordination sphere, while the core of the complex remains rather the same in both conformers $\mathbf{1^a}$ and $\mathbf{1^b}$ (Fig. 2b).

Crystal phases α and β belong to the same $P2_1/c$ space group and have similar volumes of the unit cell of about 2800 $Å^3$, which is due to the presence of the same number of crystallographically independent molecules of $\mathbf{1^a}$ that are localized on the center of inversion (Table 1). However, both polymorphs differ in the packing of molecules in the crystal lattice forming supramolecular layered structures with various orientations of clusters (Fig. 3a and b). In turn, phases β and γ represent conformational polymorphs, which adopt roughly similar packing modes of clusters but differ in the conformation of *pyret* ligands in their secondary coordination sphere, containing conformers $\mathbf{1^a}$ and $\mathbf{1^b}$, respectively (Fig. 3b and c). Furthermore, phase γ adopts a different symmetry of the crystal lattice with the non-centrosymmetric space group $Pca2_1$ (Table 1). Thus, the molecules of $\mathbf{1^b}$ are no longer located on the crystallographic inversion center, but maintain the centrosymmetric character of their molecular structure. Contrary to phase β, the unit cell of phase γ includes two crystallographically independent supramolecular layers of the cobalt clusters, which results in doubling the length of the unit cell in one direction (the *c* and *b* parameters of phase β are similar to *b* and *a* parameters of phase γ, while parameter *c* of phase γ is almost two times bigger than corresponding parameter *a* of phase β, see Table 1).

Crystal structure of 2. The molecular structure of hexameric cluster **2** contains a similar to cluster **1** parallelogram Co_6 core composed of four edge-fused μ_3-O-centered $\{Co_3\}$ triangles (Fig. 2b). This core is stabilized by six *pyret* and six acetate anions. The latter are localized around the core acting as μ_2 ligands bridging pairs of Co ions on all edges of the Co_6 parallelogram. Four *pyret* ligands adopt μ_3-$\kappa^2(O,N)$:$\kappa^1(O)$:$\kappa^1(O)$ coordination mode and are localized above and below the plane of the Co_6 core, providing central donor μ_3-O atoms for $\{Co_3\}$ triangular units. The remaining two *pyret* ligands are coordinated to the longer edges of the Co_6 parallelogram adopting μ_2-$\kappa^2(O,N)$:$\kappa^1(O)$ coordination mode. The molecular structure of **2** is centrosymmetric and contains three pairs of symmetrically equivalent Co(II) centers, each with a different coordination environment: octahedral O_6, deformed octahedral O_4N_2, and square pyramidal O_4N (for details see ESI†). The Co–O bonds are in the range of 2.003–2.208 Å. The Co–N bonds formed with the hexacoordinated Co(II) center are slightly longer (2.359 and 2.361 Å) than those bonded to the pentacoordinated Co(II) center (2.209 Å).

Open Access Article. Published on 28 March 2024. Downloaded on 1/23/2026 5:57:32 PM.
This article is licensed under a Creative Commons Attribution 3.0 Unported Licence.

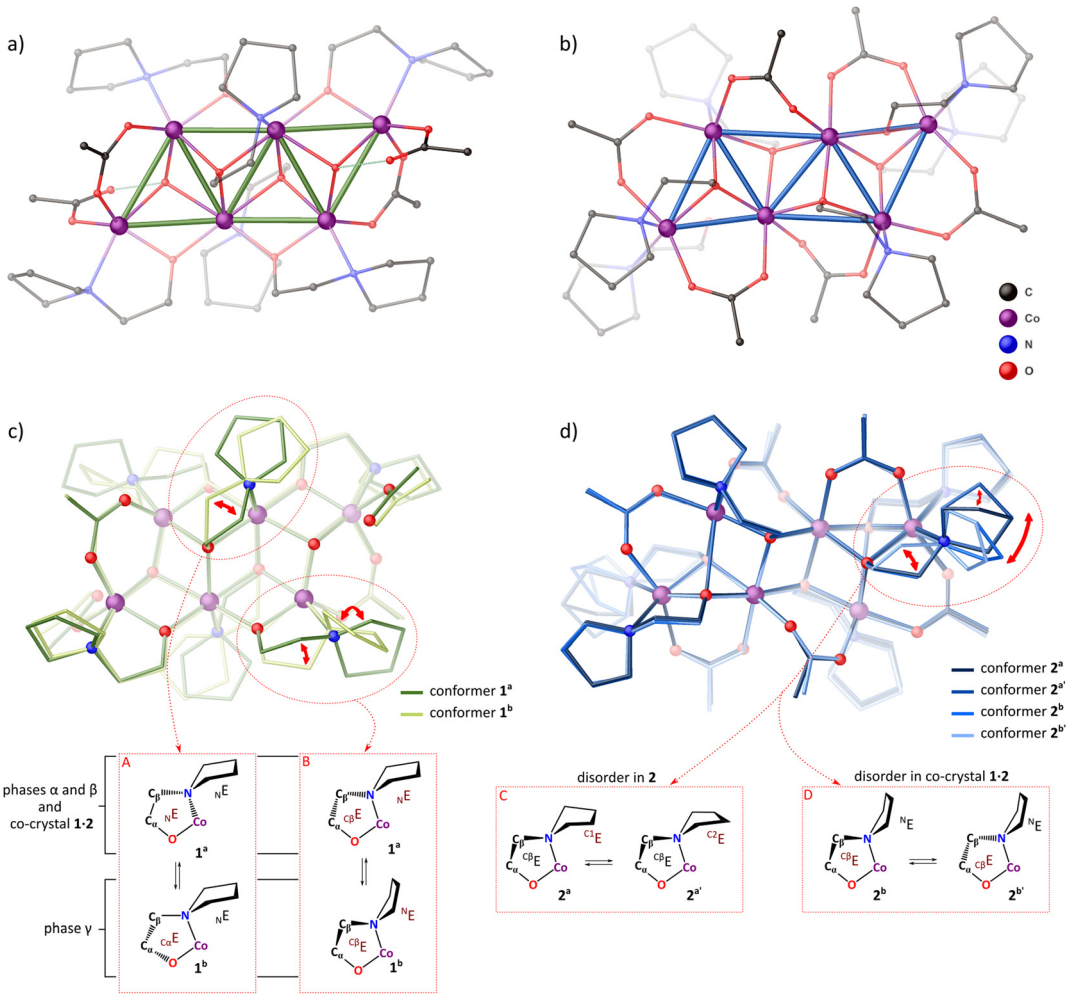

Fig. 2 Molecular structure of clusters $\mathbf{1}^{a}$ (a) and $\mathbf{2}^{a}$ (b) and main differences between their conformers (c and d). [Hydrogen atoms are omitted for clarity.]

Table 1 Selected crystallographic data for monocomponent crystals of **1** and **2** and co-crystal **1·2**

Phase *Crystal system*	**1(α)** Monoclinic	**1(β)** monoclinic	**1(γ)** orthorhombic	**2** monoclinic	**1·2** triclinic
Space group	$P2_1/n$	$P2_1/c$	$Pca2_1$	$P2_1/c$	$P\bar{1}$
Unit cell					
a (Å)	11.3990(5)	14.2057(4)	12.6327(3)	12.2702(2)	10.1181(4)
b (Å)	11.6220(6)	12.0883(4)	15.3660(3)	13.7088(3)	16.2501(6)
c (Å)	21.9920(10)	16.4530(7)	27.9274(5)	17.3126(3)	17.1906(7)
α (°)	90	90	90	90	93.061(3)
β (°)	105.784(2)	93.260(3)	90	91.439(2)	91.191(3)
γ (°)	90	90	90	90	91.462(3)
Volume (Å^3)	2803.63	2820.78	5421.1	2911.23	2820.83
Z/*Z*′/*Z*″	2/0.5	2/0.5	4/1	2/0.5	1/0.5/1
CCDC†	2321237	2321236	2321235	2321233	2321234

Cluster **2** also forms various conformers originating from the conformational movements of both the {$CoOC_{\alpha}C_{\beta}N$} macrocycles and pyrrolidine rings (Fig. 2d). Different conformers of **2** are observed in its monocomponent crystal and co-crystal **1·2** (*vide infra*), which are named $\mathbf{2}^{a}$ and $\mathbf{2}^{b}$, respectively. Interestingly, the molecular structure of $\mathbf{2}^{a}$ exhibits disorder in the position of one of the carbon atoms in pyrrolidine group of two μ_3-κ^2(*O*, *N*):κ^1(*O*):κ^1(*O*)-*pyret* ligands, which represents transitions between ^{C1}E and ^{C2}E envelope conformations of N-heterocycle (Fig. 2d, frame C). Cluster **2** crystallizes in the same $P2_1/c$ space group as phase β of **1** adopting similar crystal packing of molecules and thus similar parameters of the unit cell (see Table 1).

This journal is © The Royal Society of Chemistry 2024

Open Access Article. Published on 28 March 2024. Downloaded on 1/23/2026 5:57:32 PM.
This article is licensed under a Creative Commons Attribution 3.0 Unported Licence.

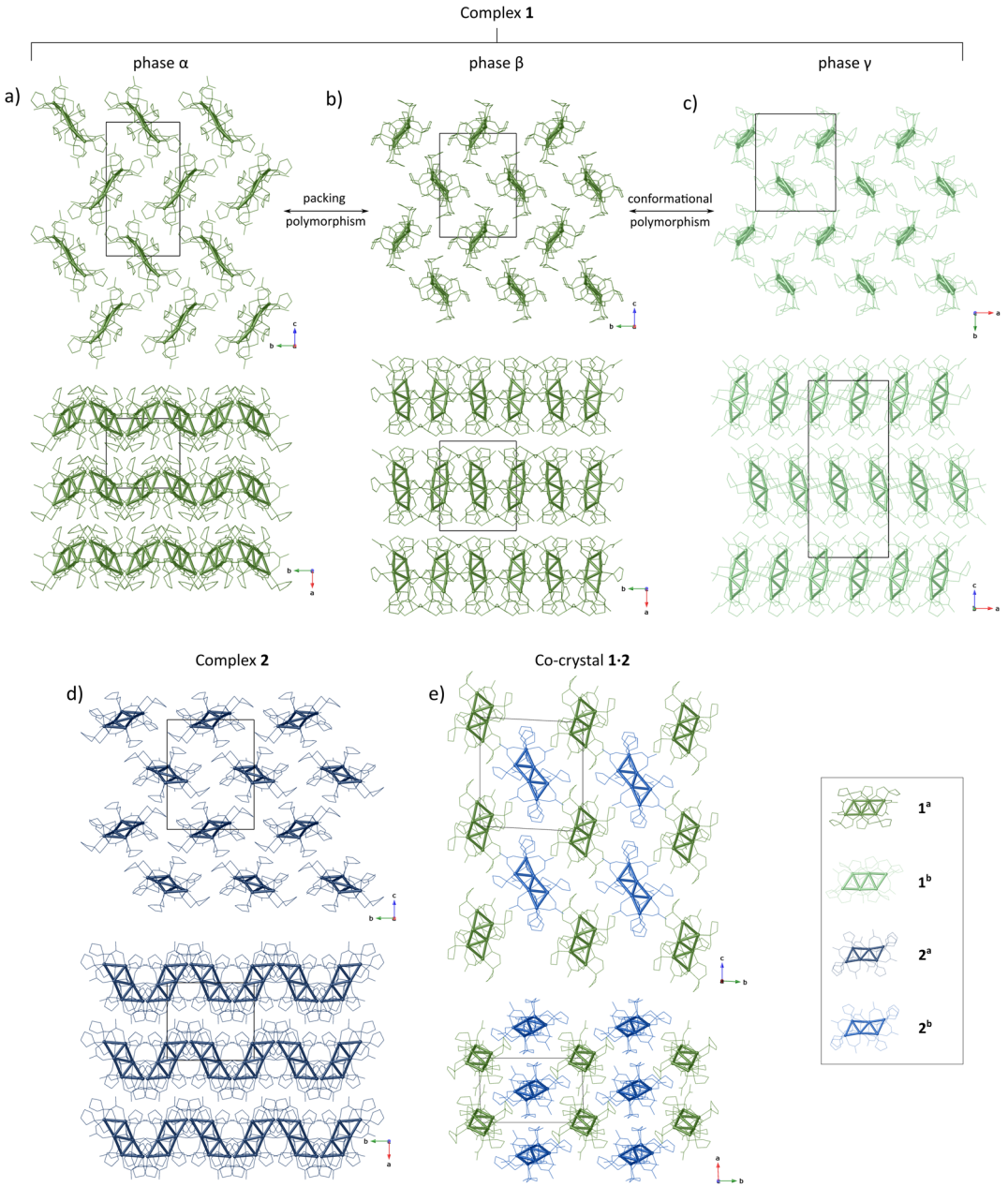

Fig. 3 Supramolecular structures of phases α, β, and γ of cluster **1**, as well as cluster **2**, and co-crystal **1·2**.

Crystal structure of co-crystal 1·2 derived from selective self-assembly of 1 and 2. The unit cell of co-crystal **1·2** contains one molecule each of complexes **1** and **2**. In this original material cluster **1** adopts conformation $\mathbf{1^a}$ similar to that observed for the polymorphic forms α and β, while cluster **2** shows conformation $\mathbf{2^b}$, which differs from that observed in the monocomponent crystal of **2** mainly by the position of N-heterocycle (Fig. 2d). Furthermore, $\mathbf{2^b}$ exhibits disorder in the position of C_β atom in the $\{CoOC_\alpha C_\beta N\}$ macrocycle formed by one of the μ_3-$\kappa^2(O,N)$:$\kappa^1(O)$:$\kappa^1(O)$-*pyret* ligands representing a transition between $^{C_\beta}$E and $_{C_\beta}$E envelope conformations (Fig. 2d, frame D). This transition is accompanied by small movements of pyrrolidine ring, which maintains the N-*exo* envelope conformation ^{N}E. The supramolecular structure of co-crystal **1·2** resembles the crystal lattice of CsCl, composed of two interpenetrated cubic arrays (Fig. 3e). In this view, the respective molecules of **1** and **2** adopt an arrangement that maximizes the contacts between various co-formers, *i.e.*, each molecule of **1** is surrounded by eight molecules of **2** and *vice versa*.

In order to more in-depth understand the propensity of clusters **1** and **2** to the selective formation of co-crystals, we performed a Hirshfeld surface examination, which is a useful tool in the analysis of crystal packing of molecules and interactions between them.[83] The analysis confirmed the prevalence of intermolecular contacts involving both co-formers in co-crystal **1·2**, which correspond to about 70% of Hirshfeld surface area for

Open Access Article. Published on 28 March 2024. Downloaded on 1/23/2026 5:57:32 PM.
This article is licensed under a Creative Commons Attribution 3.0 Unported Licence.

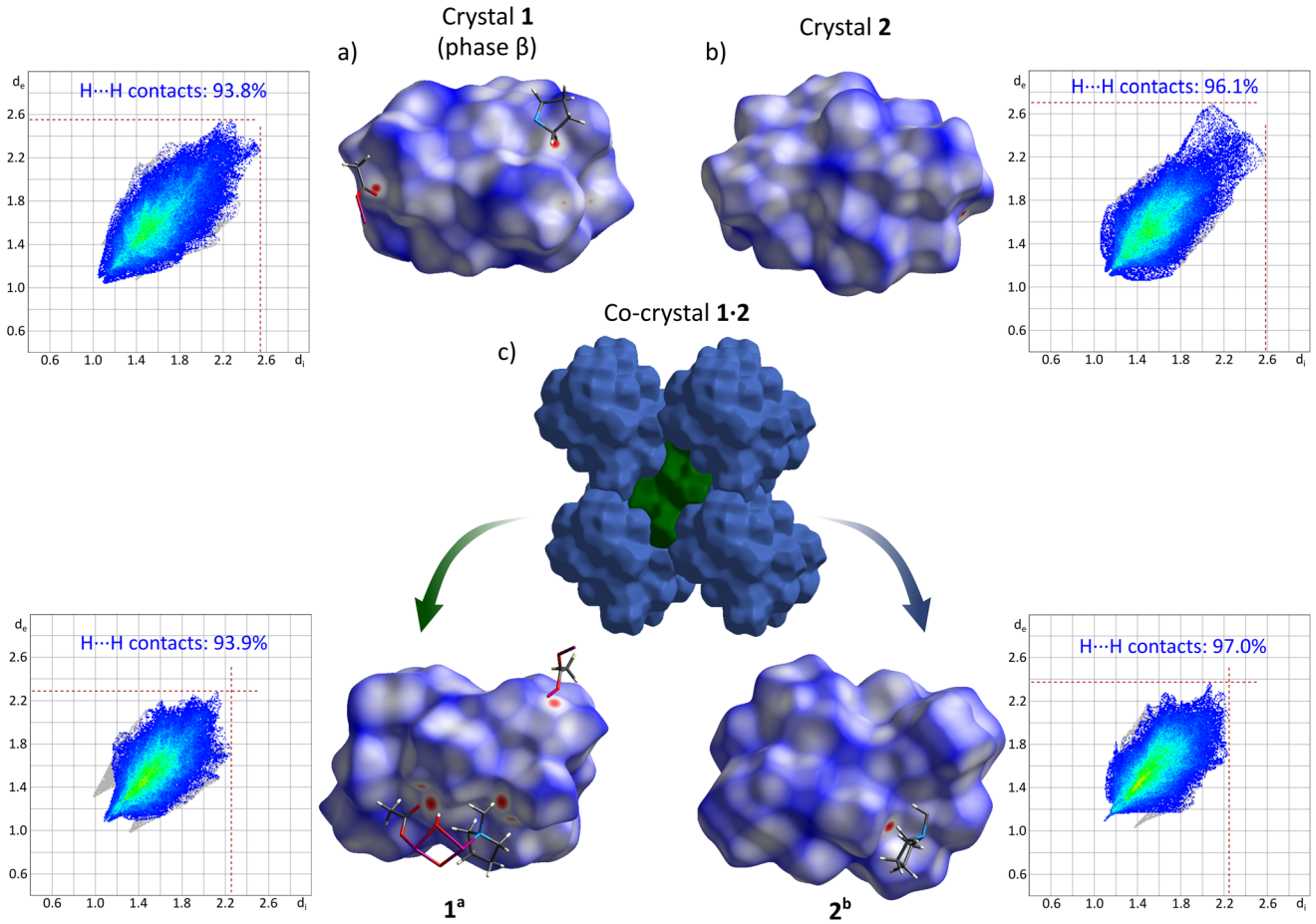

Fig. 4 Hirshfeld surfaces (mapped with d_{norm}) and fingerprint plots (d_e *vs.* d_i) of clusters **1** (phase β) and **2** in monocomponent crystals and co-crystal **1·2**.

both compounds (Fig. 4c, for details, see ESI†). Furthermore, the intermolecular contacts in all examined crystal structures of **1**, **2**, and **1·2** are significantly dominated by H···H interactions, which correspond to about 93–97% of their Hirshfeld surfaces area (Fig. 4 and ESI†). Besides that, some short intermolecular O···H distances with the lengths of 2.841(3) Å and 2.422(3)–2.567(3) Å are present in the crystal structures of phase β and co-crystal **1·2**, respectively, which may indicate the formation of intermolecular C–H···O hydrogen bonds. However, these interactions are rather weak and the self-assembly of clusters **1** and **2** is likely dominated by van der Waals forces, which rapidly weaken with the distance between atoms ($\sim 1/r^6$). Thus, the shortening of intermolecular contacts significantly strengthens the interactions between molecules. Analysis of contact distances on the Hirshfeld surface shows that the clusters are more compactly packed in co-crystal **1·2** than in monocomponent crystals of individual co-formers. For instance, distances from the Hirshfeld surface of cluster **1** to the nearest interior (d_i) and exterior (d_e) atoms are in the ranges of 1.048–2.555 Å and 1.046–2.563 Å in phase β and only 0.995–2.293 Å and 0.995–2.349 Å in co-crystal **1·2** (Fig. 4a, c and Table S8†). Similarly, the d_i and d_e values for cluster **2** are in the ranges of 1.062–2.593 Å and 1.061–2.703 Å and only 1.096–2.271 Å and 1.035–2.367 Å in monocomponent crystal **2** and co-crystal **1·2**, respectively (Fig. 4b, c and Table S8†). This indicates on unique mutual shape complementarity of both clusters, which combined with the high adaptability of their flexible secondary coordination sphere leads to efficient tight packing of moleules in the multicomponent crystals. The shortening of intermolecular contacts between clusters enhances van der Waals interactions between them, which likely drives the selective formation of stoichiometric co-cocrystals instead of a mixture of monocomponent crystals.

Conclusion

In summary, on the example of heteroleptic Co(II) carboxylato clusters we are tackling three issues of general importance for inorganic synthesis and crystal engineering: (i) the role of proper purification of starting reagents, (ii) both packing and conformational polymorphism in organic–inorganic molecular building units, and (iii) their selective co-crystallization. Particularly, we revealed that the commonly used thermal procedure for dehydration of cobalt(II) acetate leads to a reagent comprising substantial contamination by cobalt hydroxido moieties. Hence, we developed a new approach for the successful

 This journal is © The Royal Society of Chemistry 2024

Open Access Article. Published on 28 March 2024. Downloaded on 1/23/2026 5:57:32 PM. This article is licensed under a Creative Commons Attribution 3.0 Unported Licence.

dehydration of cobalt(II) acetate by the application of acetic anhydride, which will help prevent accidental contaminations of reaction systems in the future. Utilizing both reagents we obtained two new heteroleptic hydroxido-acetato and acetato Co(II) clusters **1** and **2**, respectively, incorporating auxiliary *O,N*-bidentate *pyret* ligands. A comprehensive structural examination of **1** revealed the intriguing diversity of its crystal structure, which represents a rare example of both conformational and packing polymorphism in one compound, originating from the flexibility of organic *O,N*-ligands in the secondary coordination sphere. In the next control experiment, we revealed the propensity of clusters **1** and **2** for the formation of co-crystals with 1 : 1 stoichiometry. Remarkably, the selective self-assembly of both compounds is driven mainly by van der Waals forces, which indicates that their shape complementarity and secondary coordination sphere adaptivity are the main factors leading to the selective formation of multicomponent crystals **1·2**. This is in contrast to the majority of previously reported co-crystals, which were usually organized *via* specific complementary intermolecular interactions like hydrogen or halogen bonds.[35,39,49,61]

Experimental section

Materials and methods

All manipulations were conducted under a dry, oxygen-free argon atmosphere either using standard Schlenk techniques or in a glovebox. All reagents were purchased from commercial vendors: *pyret*-H (Sigma-Aldrich), KHMDS (Sigma-Aldrich), acetic anhydride (Sigma-Aldrich), cobalt(II) acetate (Sigma-Aldrich), cobalt(II) chloride (ABCR). *pyret*-H was purified by distillation over CaH_2 under an argon atmosphere. Other reagents were used as received and stored/manipulated in a glovebox. Solvents were purified using an MBraun SPS-5 system.

IR spectroscopy

FTIR spectra were measured with a Bruker Tensor II spectrometer using the ATR technique.

Elemental analysis

Elemental CHN + O analyses were performed using a UNICUBE elemental analyzer (Elementar Analysensysteme GmbH). The Co content was determined using the ICP-OES spectrometer Shimadzu ICPE-9820.

TGA analysis

TGA was carried out with a TA Instruments Q600 instrument under an Ar flow (flow rate of 100 mL min^{-1}) to 600 °C at a heating rate of 5 °C min^{-1}.

Powder X-ray diffraction

PXRD data were collected with an Empyrean diffractometer (PANalytical) by employing Ni-filtered CuKα radiation from a copper sealed tube charged with 40 kV voltage and 40 mA current in Bragg–Brentano geometry with a beam divergence of 1° in the scattering plane.

Single-crystal X-ray diffraction

The crystals were selected under Paratone-N oil, mounted on the nylon loops, and positioned in the cold stream on the diffractometer. The X-ray data for complexes **1(β)**, **1(γ)**, **2**, and **1·2**, were collected at 100(2) K on a SuperNova Agilent diffractometer using graphite monochromated MoKα radiation (λ = 0.71073 Å). The data were processed with CrysAlisPro.[84] The X-ray data for complex **1(α)** was collected at 100(2) K on a Nonius Kappa CCD diffractometer[85] using graphite monochromated MoKα radiation (λ = 0.71073 Å). The unit cell parameters were determined from ten frames and then refined on all data. The data were processed with DENZO and SCALEPACK (HKL2000 package).[86] The crystal structures were solved by direct methods using the SHELXS-97 program and were refined by full-matrix least-squares on F2 using the program SHELXL[87] implemented in the Olex2[88] or WinGX[89] suite. All non-hydrogen atoms were refined with anisotropic displacement parameters. Hydrogen atoms were added to the structure model in geometrically idealized coordinates and further refined as riding atoms in addition to the H6 and H12 hydrogen atoms in the **1(γ)** molecule. The H atoms of the hydroxyl groups were located based on the electron density map and refined with constraints at O–H distances of 0.980(2) Å. Details of structure refinements and crystal data are provided in ESI.† Crystallographic data have been deposited with the Cambridge Crystallographic Data Centre, CCDC 2321237 (**1α**), 2321236 (**1β**), 2321235 (**1γ**), 2321233 (**2**), 2321234 (**1·2**).†

Hirshfeld surface analysis was carried out based on molecular geometries from the X-ray crystal structures using the program CrystalExplorer 17.5.[90]

The coordination sphere geometry of Co(II) centers in the presented structures was analyzed employing the continuous shape measurement (CShM)[91] using SHAPE software.[92] The results are presented in Tables S6 and S7 in ESI.†

Synthesis and characterization

Purification of $Co(OAc)_2$. *Thermal procedure*: commercial $Co(OAc)_2{\cdot}4H_2O$ (2 g) was heated at 120 °C under reduced pressure by 12 h, which led to a color change from pink to purple. The resulting product was characterized by elemental analysis and compared with commercial anhydrous $Co(OAc)_2$. Elemental analysis: for *thermally treated Co(OAc)$_2$*: calcd (%) for $[Co(OH)_{0.28}(OAc)_{1.72}]{\cdot}0.12H_2O$ ($C_{3.44}H_{5.68}O_{3.84}Co_1$) (167.41): C 24.68; H 3.42; O 36.70; Co 35.20. Found (%): C 24.70; H 3.14; O 36.77; Co 35.07.

For *commertial Co(OAc)$_2$*: calcd (%) for $[Co(OH)_{0.34}(OAc)_{1.66}]{\cdot}0.70H_2O$, ($C_{3.32}H_{6.72}O_{4.36}Co_1$) (175.34): C 22.74; H 3.86; O 39.78; Co 33.61. Found (%): C 22.79; H 3.91; O 39.76; Co 33.35.

Acetic anhydride procedure: commercial anhydrous $Co(OAc)_2$ or $Co(OAc)_2{\cdot}4H_2O$ (2 g) was added to a flask containing 50 ml of acetic anhydride and stirred for 24 h at 90 °C. Then the excess liquid was distilled under reduced pressure and the residual pink powder was dried under vacuum. Elemental analysis: calcd (%) for $Co(OAc)_2$ ($C_4H_6O_4Co_1$) (177.01): C 27.14; H 3.42; O 36.15; Co 33.28. Found (%): C 27.35; H 3.64; O 35.48; Co 33.36.

Open Access Article. Published on 28 March 2024. Downloaded on 1/23/2026 5:57:32 PM. This article is licensed under a Creative Commons Attribution 3.0 Unported Licence.

Synthesis of *pyret*-K. An equimolar amount of *pyret*-H (871 mg, 10 mmol) was added to a Schlenk flask containing KHMDS (1995 mg, 10 mmol) dispersed in hexane (50 ml). The reaction was stirred for 24 h. The resulting white suspension was filtered, washed two times with hexane, and dried under vacuum leading to *pyret*-K in essentially quantitative yield.

Synthesis of 1. An equimolar amount of commercial or thermally treated $Co(OAc)_2$ (177 mg, 1 mmol) was added to a suspension of *pyret*-K (153 mg, 1 mmol) in THF. The reaction was stirred for 24 h. The product was isolated as violet-pink crystals after filtration and crystallization in the presence of hexane vapor at room temperature (yield = 89%, 170 mg). Alternatively, in the reaction, purified $Co(OAc)_2$ (177 mg, 1 mmol) may be used followed by the addition of 0.3 equivalent water (2 M in THF, 0.15 ml) leading to the same product (yield = 80%, 152 mg). IR(ATR): ν/cm^{-1} 3292 (bw), 2975 (m), 2934 (m), 2878 (m), 2826 (m), 1586 (s), 1432 (s), 1424 (s), 1101 (m), 1073 (s), 958 (m), 946 (m), 900 (m), 661 (m), 609 (m), 457 (s). Elemental analysis: calcd (%) for $[Co_6(OH)_2(OAc)_4(pyret)_6]$ ($C_{32}H_{62}N_6O_{16}Co_6$) (1140.45): C 33.70; H 5.47; N 7.37, O 22.45. Found (%): C 33.89; H 5.86; N 7.36, O 22.88.

Synthesis of 2. An equimolar amount of purified $Co(OAc)_2$ (177 mg, 1 mmol) was added to a suspension of *pyret*-K (153 mg, 1 mmol) in 5 ml THF. The reaction was stirred for 24 h. The product was isolated as violet-pink crystals after filtration and crystallization in the presence of hexane vapor at room temperature (yield = 75%, 150 mg). IR(ATR): ν/cm^{-1} 2975 (m), 2934 (m), 2878 (m), 2826 (s), 1590 (s), 1578 (s), 1418 (s), 1101 (m), 1073 (s), 1065 (s), 958 (s), 946 (s), 884 (s), 661 (s), 615 (s), 457 (m). Elemental analysis: calcd (%) for $[Co_6(OAc)_6(pyret)_6]$ ($C_{36}H_{66}N_6O_{18}Co_6$) (1224.53): C 35.31; H 5.43; N 6.86, O 23.52. Found (%): C 35.77; H 5.46; N 6.57, O 23.49.

Synthesis of co-crystals 1·2

Method 1. $CoCl_2$ (65 mg, 0.5 mmol) was added to a suspension of 2 equivalents of *pyret*-K (153 mg, 1 mmol) in THF (7 ml). The reaction was stirred for 24 h. Then, the commercial $Co(OAc)_2$ (177 mg, 1 mmol) was added to the resulting violet solution of $[Co(pyret)_2]$ and stirred for another 24 h. The product was isolated as violet-pink crystals after filtration and crystallization in the presence of hexane vapor at room temperature (yield = 86%, 250 mg).

Method 2. Equimolar amounts of **1** (114 mg, 0.1 mmol) and **2** (122 mg, 0.1 mmol) were slowly dissolved in THF (10 ml). The product was isolated as violet-pink crystals after filtration and crystallization in the presence of hexane vapor at room temperature (yield = 79%, 186 mg).

Elemental analysis: calcd (%) for $[Co_6(OH)_2(OAc)_4(pyret)_6]\cdot[Co_6(OAc)_6(pyret)_6]$ ($C_{68}H_{128}N_{12}O_{34}Co_{12}$) (2364.98): C 34.54; H 5.46; N 7.11, O 23.00. Found (%): C 34.55; H 5.59; N 7.02, O 23.34.

Conflicts of interest

There are no conflicts to declare.

Acknowledgements

The authors acknowledge the National Science Centre (Grant PRELUDIUM 2018/29/N/ST5/02377) for financial support.

References

1 I. E. Jacobs and A. J. Moulé, *Adv. Mater.*, 2017, **29**, 1–39.
2 A. Ghosh, O. F. Mohammed and O. M. Bakr, *Acc. Chem. Res.*, 2018, **51**, 3094–3103.
3 G. R. Fulmer, A. J. M. Miller, N. H. Sherden, H. E. Gottlieb, A. Nudelman, B. M. Stoltz, J. E. Bercaw and K. I. Goldberg, *Organometallics*, 2010, **29**, 2176–2179.
4 A. Y. Rulev, *New J. Chem.*, 2017, **41**, 4262–4268.
5 L. M. Liz-Marzán, C. R. Kagan and J. E. Millstone, *ACS Nano*, 2020, **14**, 6359–6361.
6 *History of polyilefines*, ed. R. B. Seymour and T. Cheng, D. Reidel Publishing Company, Dordrech, 1986.
7 H. Werner, *Angew. Chem., Int. Ed.*, 2012, **51**, 6052–6058.
8 K. Yu and K. S. Schanze, *ACS Cent. Sci.*, 2023, **9**, 1989–1992.
9 R. G. Bergman and R. L. Danheiser, *Angew. Chem., Int. Ed.*, 2016, **55**, 12548–12549.
10 T. Schnitzer, M. D. Preuss, J. van Basten, S. M. C. Schoenmakers, A. J. H. Spiering, G. Vantomme and E. W. Meijer, *Angew. Chem., Int. Ed.*, 2022, **61**, e202206738.
11 W. L. F. Armarego and C. L. L. Chai, *Purification of Laboratory Chemicals*, Elsevier, 2009.
12 D. Tilly, G. Dayaker and P. Bachu, *Catal. Sci. Technol.*, 2014, **4**, 2756–2777.
13 G. S. S. Treesa, M. Neetha, S. Saranya and G. Anilkumar, *ChemistrySelect*, 2020, **5**, 7400–7416.
14 M. Smyrnioti and T. Ioannides, in *Cobalt*, InTech, 2017.
15 F. H. Wei, D. Chen, Z. Liang, S. Q. Zhao and Y. Luo, *RSC Adv.*, 2017, **7**, 46520–46528.
16 R. K. Tripathy, A. K. Samantara and J. N. Behera, *Dalton Trans.*, 2019, **48**, 10557–10564.
17 S. Aryanejad, G. Bagherzade and M. Moudi, *Appl. Organomet. Chem.*, 2019, **33**, 1–11.
18 M. Murrie, *Chem. Soc. Rev.*, 2010, **39**, 1986–1995.
19 A. J. Ward, A. F. Masters and T. Maschmeyer, in *Comprehensive Inorganic Chemistry II*, Elsevier, 2013, pp. 191–228.
20 A. J. Ward, A. F. Masters and T. Maschmeyer, in *Comprehensive Inorganic Chemistry II*, Elsevier, 2013, pp. 665–684.
21 J. J. R. Fraústo da Silva and R. J. P. Williams, *The Biological Chemistry of the Elements, The Inorganic Chemistry of Life*, Oxford University Press, 2001.
22 N. Mitić, S. J. Smith, A. Neves, L. W. Guddat, L. R. Gahan and G. Schenk, *Chem. Rev.*, 2006, **106**, 3338–3363.
23 Z. Tomkowicz, S. Ostrovsky, S. Foro, V. Calvo-Perez and W. Haase, *Inorg. Chem.*, 2012, **51**, 6046–6055.
24 S. Durot, C. Policar, G. Pelosi, F. Bisceglie, T. Mallah and J. P. Mahyt, *Inorg. Chem.*, 2003, **42**, 8072–8080.

 This journal is © The Royal Society of Chemistry 2024

Open Access Article. Published on 28 March 2024. Downloaded on 1/23/2026 5:57:32 PM. This article is licensed under a Creative Commons Attribution 3.0 Unported Licence.

25 L. Cañadillas-Delgado, O. Fabelo, J. Pasán, F. S. Delgado, F. Lloret, M. Julve and C. Ruiz-Pérez, *Inorg. Chem.*, 2007, **46**, 7458–7465.
26 M. Zhao, H. B. Wang, L. N. Ji and Z. W. Mao, *Chem. Soc. Rev.*, 2013, **42**, 8360–8375.
27 C. Van Stappen, Y. Deng, Y. Liu, H. Heidari, J. X. Wang, Y. Zhou, A. P. Ledray and Y. Lu, *Chem. Rev.*, 2022, **122**, 11974–12045.
28 G. Aromí, A. S. Batsanov, P. Christian, M. Helliwell, A. Parkin, S. Parsons, A. A. Smith, G. A. Timco and R. E. P. Winpenny, *Chem. - Eur. J.*, 2003, **9**, 5142–5161.
29 G. E. Kostakis, S. P. Perlepes, V. A. Blatov, D. M. Proserpio and A. K. Powell, *Coord. Chem. Rev.*, 2012, **256**, 1246–1278.
30 A. J. Cruz-Cabeza and J. Bernstein, *Chem. Rev.*, 2014, **114**, 2170–2191.
31 A. J. Cruz-Cabeza, S. M. Reutzel-Edens and J. Bernstein, *Chem. Soc. Rev.*, 2015, **44**, 8619–8635.
32 Y. Zhou, J. Wang, Y. Xiao, T. Wang and X. Huang, *Curr. Pharm. Des.*, 2018, **24**, 2375–2382.
33 G. C. Zimmer, A. B. Pagliari, V. B. Solner, M. Hörner, H. G. Bonacorso, N. Zanatta and M. A. P. Martins, *Cryst. Growth Des.*, 2021, **21**, 4690–4706.
34 N. Shan and M. J. Zaworotko, *Drug Discovery Today*, 2008, **13**, 440–446.
35 D. Braga, L. Maini and F. Grepioni, *Chem. Soc. Rev.*, 2013, **42**, 7638.
36 S. Aitipamula, P. S. Chow and R. B. H. Tan, *CrystEngComm*, 2014, **16**, 3451–3465.
37 S. Cherukuvada, R. Kaur and T. N. Guru Row, *CrystEngComm*, 2016, **18**, 8528–8555.
38 E. Grothe, H. Meekes, E. Vlieg, J. H. ter Horst and R. de Gelder, *Cryst. Growth Des.*, 2016, **16**, 3237–3243.
39 C. A. Gunawardana and C. B. Aakeröy, *Chem. Commun.*, 2018, **54**, 14047–14060.
40 X. Kang and M. Zhu, *ACS Mater. Lett.*, 2020, **2**, 1303–1314.
41 M. Bodiuzzaman, W. A. Dar and T. Pradeep, *Small*, 2021, **17**, 1–15.
42 J. J. Jiang, M. Pan, J. M. Liu, W. Wang and C. Y. Su, *Inorg. Chem.*, 2010, **49**, 10166–10173.
43 D. Aulakh, J. R. Varghese and M. Wriedt, *Inorg. Chem.*, 2015, **54**, 8679–8684.
44 Y. Huang, Z. Wang, Z. Chen and Q. Zhang, *Angew. Chem., Int. Ed.*, 2019, **58**, 9696–9711.
45 L. Sun, Y. Wang, F. Yang, X. Zhang and W. Hu, *Adv. Mater.*, 2019, **31**, 1–22.
46 X. Kang and M. Zhu, *Chem. Soc. Rev.*, 2019, **48**, 2422–2457.
47 D. Gentili, M. Gazzano, M. Melucci, D. Jones and M. Cavallini, *Chem. Soc. Rev.*, 2019, **48**, 2502–2517.
48 H. Bergeron, D. Lebedev and M. C. Hersam, *Chem. Rev.*, 2021, **121**, 2713–2775.
49 L. Sun, W. Zhu, X. Zhang, L. Li, H. Dong and W. Hu, *J. Am. Chem. Soc.*, 2021, **143**, 19243–19256.
50 M. J. De Velásquez-Hernández, A. Torres-Huerta, D. Martínez-Otero, E. Sánchez-González, U. Hernández-Balderas, I. A. Ibarra and V. Jancik, *Cryst. Growth Des.*, 2018, **18**, 3805–3819.
51 Q. Chen, T. Zhang, X. Chen, M. Liang, H. Zhao, P. Yuan, Y. Han, C. P. Li, J. Hao and P. Xue, *ACS Appl. Mater. Interfaces*, 2022, **14**, 24509–24517.
52 T. Hashimoto, R. Oketani, M. Nobuoka, S. Seki and I. Hisaki, *Angew. Chem., Int. Ed.*, 2023, **62**, 1–6.
53 J. C. Christopherson, F. Topić, C. J. Barrett and T. Friščić, *Cryst. Growth Des.*, 2018, **18**, 1245–1259.
54 M. P. Zhuo, Y. C. Tao, X. D. Wang, Y. Wu, S. Chen, L. S. Liao and L. Jiang, *Angew. Chem., Int. Ed.*, 2018, **57**, 11300–11304.
55 H. Jain, D. Sutradhar, S. Roy and G. R. Desiraju, *Angew. Chem., Int. Ed.*, 2021, **60**, 12841–12846.
56 J. T. A. Jones, T. Hasell, X. Wu, J. Bacsa, K. E. Jelfs, M. Schmidtmann, S. Y. Chong, D. J. Adams, A. Trewin, F. Schiffman, F. Cora, B. Slater, A. Steiner, G. M. Day and A. I. Cooper, *Nature*, 2011, **474**, 367–371.
57 M. Liu, L. Zhang, M. A. Little, V. Kapil, M. Ceriotti, S. Yang, L. Ding, D. L. Holden, R. Balderas-Xicohténcatl, D. He, R. Clowes, S. Y. Chong, G. Schütz, L. Chen, M. Hirscher and A. I. Cooper, *Science*, 2019, **366**, 613–620.
58 L. K. Das, A. Biswas, C. J. Gómez-García, M. G. B. Drew and A. Ghosh, *Inorg. Chem.*, 2014, **53**, 434–445.
59 D. Braga, F. Grepioni and O. Shemchuk, *CrystEngComm*, 2018, **20**, 2212–2220.
60 V. Nemec, K. Lisac, N. Bedeković, L. Fotović, V. Stilinović and D. Cinčić, *CrystEngComm*, 2021, **23**, 3063–3083.
61 N. A. Mir, R. Dubey and G. R. Desiraju, *Acc. Chem. Res.*, 2019, **52**, 2210–2220.
62 J. Lewiński, W. Bury, M. Dutkiewicz, M. Maurin, I. Justyniak and J. Lipkowski, *Angew. Chem., Int. Ed.*, 2008, **47**, 573–576.
63 W. Bury, I. Justyniak, D. Prochowicz, A. Rola-Noworyta and J. Lewiński, *Inorg. Chem.*, 2012, **51**, 7410–7414.
64 K. Sokołowski, W. Bury, I. Justyniak, D. Fairen-Jimenez, K. Sołtys, D. Prochowicz, S. Yang, M. Schröder and J. Lewiński, *Angew. Chem.*, 2013, **125**, 13656–13660.
65 K. Sokołowski, I. Justyniak, W. Bury, J. Grzonka, Z. Kaszkur, Ł. Mąkolski, M. Dutkiewicz, A. Lewalska, E. Krajewska, D. Kubicki, K. Wójcik, K. J. Kurzydłowski and J. Lewiński, *Chem. – Eur. J.*, 2015, **21**, 5488–5495.
66 M. K. Leszczyński, I. Justyniak, K. Zelga and J. Lewiński, *Dalton Trans.*, 2017, **46**, 12404–12407.
67 J. Nawrocki, D. Prochowicz, I. Justyniak, J. van Leusen, A. Kornowicz, P. Kögerler and J. Lewiński, *Dalton Trans.*, 2019, **48**, 12828–12831.
68 P. Krupiński, M. Terlecki, A. Kornowicz, I. Justyniak, D. Prochowicz, J. van Leusen, P. Kögerler and J. Lewiński, *Inorg. Chem.*, 2022, **61**, 7869–7877.
69 V. Gupta, I. Justyniak, E. Chwojnowska, V. Szejko and J. Lewiński, *Inorg. Chem.*, 2023, **62**, 16274–16279.
70 T. Kaczorowski, I. Justyniak, T. Lipińska, J. Lipkowski and J. Lewiński, *J. Am. Chem. Soc.*, 2009, **131**, 5393–5395.
71 J. Lewiński, T. Kaczorowski, D. Prochowicz, T. Lipińska, I. Justyniak, Z. Kaszkur and J. Lipkowski, *Angew. Chem., Int. Ed.*, 2010, **49**, 7035–7039.

Open Access Article. Published on 28 March 2024. Downloaded on 1/23/2026 5:57:32 PM.
This article is licensed under a Creative Commons Attribution 3.0 Unported Licence.

72 M. Terlecki, S. Sobczak, M. K. Leszczyński, A. Katrusiak and J. Lewiński, *Chem. - Eur. J.*, 2021, **27**, 13757–13764.
73 M. Terlecki, I. Justyniak, M. K. Leszczyński and J. Lewiński, *Commun. Chem.*, 2021, **4**, 133.
74 A. Kornowicz, M. Terlecki, I. Justyniak, D. Prochowicz, J. Van Leusen, P. Kögerler and J. Lewiński, *Inorg. Chem.*, 2022, **61**, 2499–2508.
75 A. Kornowicz, M. Terlecki, D. Prochowicz, C. Pichon, I. Justyniak, W. Bury, Z. Wróbel, J.-P. Sutter and J. Lewiński, *Eur. J. Inorg. Chem.*, 2017, **2017**, 1392–1395.
76 K. Korona, M. Terlecki, I. Justyniak, M. Magott, J. Żukrowski, A. Kornowicz, D. Pinkowicz, A. Kubas and J. Lewiński, *Chem. - Eur. J.*, 2022, **28**, e202200620.
77 G. Zhang, J. Lin, D. Guo, S. Yao and Y. Tian, *Z. Anorg. Allg. Chem.*, 2010, **636**, 1401–1404.
78 K. Nagase, H. Yokobayashi and K. Sone, *Bull. Chem. Soc. Jpn.*, 1976, **49**, 1563–1567.
79 V. Pock, *Encyclopedia of Reagents for Organic Synthesis*, Wiley, 2001, vol. 1996.
80 E. Ingier-Stocka and A. Grabowska, *J. Therm. Anal. Calorim.*, 1998, **54**, 115–123.
81 R. Kuhlman, G. L. Schimek and J. W. Kolis, *Inorg. Chem.*, 1999, **38**, 194–196.
82 H. Satoh and S. Manabe, *Chem. Soc. Rev.*, 2013, **42**, 4297.
83 M. A. Spackman and D. Jayatilaka, *CrystEngComm*, 2009, **11**, 19–32.
84 *CrysAlisPro 1.171.38.41*, Rigaku Oxford Diffraction; Rigaku Corp. Oxford, UK.
85 *KappaCCD Software*, Nonius B. V., Delft, The Netherlands, 1998.
86 Z. Otwinowski and W. Minor, in *Methods in Enzymology*, 1997, vol. 276, pp. 307–326.
87 G. M. Sheldrick, *Acta Crystallogr., Sect. C: Struct. Chem.*, 2015, **71**, 3–8.
88 L. J. Bourhis, O. V. Dolomanov, R. J. Gildea, J. A. K. Howard and H. Puschmann, *Acta Crystallogr., Sect. A: Found. Adv.*, 2015, **71**, 59–75.
89 L. J. Farrugia, *J. Appl. Crystallogr.*, 2012, **45**, 849–854.
90 P. R. Spackman, M. J. Turner, J. J. McKinnon, S. K. Wolff, D. J. Grimwood, D. Jayatilaka and M. A. Spackman, *J. Appl. Crystallogr.*, 2021, **54**, 1006–1011.
91 H. Zabrodsky, S. Peleg and D. Avnir, *J. Am. Chem. Soc.*, 1992, **114**, 7843–7851.
92 M. Llunell, D. Casanova, J. Cirera, P. Alemany and S. Alvarez, *Version 2.1*, 2013.

This journal is © The Royal Society of Chemistry 2024